ACS central science

Research Article

Cite This: ACS Cent. Sci. 2019, 5, 1059−1066

http://pubs.acs.org/journal/acscii

In Vivo Multicolor Imaging with Fluorescent Probes Revealed the Dynamics and Function of Osteoclast Proton Pumps

Masafumi Minoshima,[†] Junichi Kikuta,[‡,§] Yuta Omori,[†] Shigeto Seno,[∥] Riko Suehara,[‡] Hiroki Maeda,[†] Hideo Matsuda,[∥] Masaru Ishii,[‡,§] and Kazuya Kikuchi*[,†,§]

[†]Department of Material and Life Science, Graduate School of Engineering, Osaka University, Suita, Osaka 565-0871, Japan

[‡]Department of Immunology and Cell Biology, Graduate School of Medicine and Frontier Biosciences, Osaka University, Suita, Osaka 565-0871, Japan

[§]WPI—Immunology Frontier Research Center, Osaka University, Suita, Osaka 565-0871, Japan

[∥]Department of Bioinformatic Engineering, Graduate School of Information Science and Technology, Osaka University, Suita, Osaka 565-0871, Japan

Supporting Information

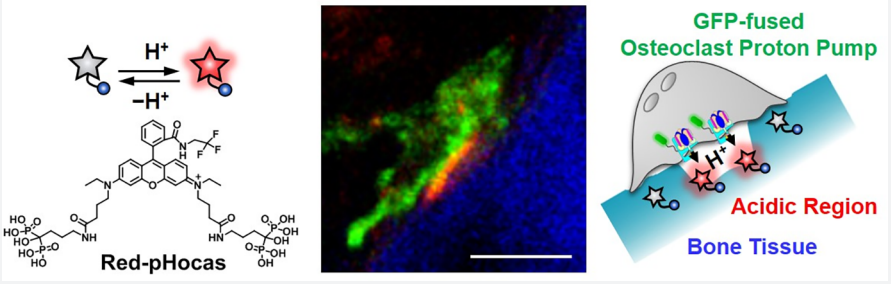

ABSTRACT: *In vivo* two-photon fluorescence imaging is a powerful modality to monitor cell dynamics in biomedical studies. To detect protein functions in living animals in real-time, fluorescent probes must show a quick response to the target function in specific tissues. Here, we developed a rhodamine-based small-molecule fluorescent probe called Red-pHocas (red pH-activatable fluorescent probe for osteoclast activity sensing) to reversibly detect the acidic environments for the spatiotemporal analysis of the function of osteoclast proton pumps. The introduction of electron-withdrawing *N*-alkyl substituents in the rhodamine spirolactam fluorophore remarkably increased the kinetics of the fluorescence response to acidic pHs, which allowed the rapid and reversible monitoring of acidic compartments and the analysis of the dynamics of osteoclast proton pumps during osteoclastic bone resorption. *In vivo* multicolor two-photon imaging using Red-pHocas in fluorescent reporter mice revealed that bone acidification occurred synchronously with the accumulation of proton pumps onto the bone surfaces. To our knowledge, this is the first study to demonstrate the direct involvement of osteoclast proton pumps in bone acidification under intravital conditions by means of an imaging probe.

INTRODUCTION

Molecular imaging is an indispensable tool to directly obtain dynamics on molecular processes *in vivo*. Among the imaging modalities, fluorescence imaging with a two-photon microscopy allows the visualization of intact cells deep within the tissues and organs with high temporal and subcellular resolutions, which contributes to the biomedical studies and clinical diagnosis.[1] Recent approaches in two-photon imaging emphasize the analyses of individual cell dynamics,[2−6] cell−cell interactions,[7−9] and drug responses in intact tissues.[10] By using fluorescently labeled agents such as genetically encoded fluorescent proteins and fluorophore-conjugated antibodies, the target cells can be visualized for tracking the locations and motilities.

In addition, *in vivo* imaging analysis of protein function is essential to explore how proteins work in maintaining the cellular and organ physiology at a molecular level over time and place. At present, limited protein function was imaged as enzyme activities such as kinases in signaling pathways and caspases in apoptotic events via fluorescent protein-based sensors.[11,12] Moreover, development of the protein-based sensors generally requires time-consuming procedures for optimization of the sensing properties and construction of the corresponding mouse models, which impose substantial hurdles for imaging applications.

Small-molecule-based fluorescent probes are promising tools as their fluorescence-sensing properties can be tuned for the optimization of their biomolecular functions and facile administration by injection.[13] For longitudinal monitoring of the protein functions in real-time with high signal/background contrast, the fluorescent probes must have a quick response and

Received: March 5, 2019
Published: May 1, 2019

DOI: 10.1021/acscentsci.9b00220
ACS Cent. Sci. 2019, 5, 1059−1066

specificity to the target function and must be photostable. In addition, efficient delivery of the probes to the target tissues is necessary for *in vivo* applications. Therefore, small-molecular probes face stringent design constraints for *in vivo* imaging applicable to the functional analysis of proteins. We previously developed a small-molecular probe for detecting the activity of bone-resorbing osteoclasts in living animals.[14,15] Osteoclasts play an essential role in regulating bone homeostasis, and disruption of the balance caused by aberrant osteoclast activity results in enhancement or reduction of bone mass, leading to bone diseases such as osteopetrosis and osteoporosis.[16,17] Using a pH-activatable BODIPY-based (BODIPY, boron-dipyrromethene) green fluorescent probe, the activity and dynamics of bone-resorbing osteoclasts were imaged for a prolonged period of time.[15] The peptide-based fluorescent probe has been developed to target upregulated cathepsin K activity of osteoclasts,[18] yet it has not been applied to real-time *in vivo* imaging.

Herein, we present multicolor intravital imaging to reveal the protein functions associated with osteoclastic bone resorption using a pH-activatable small-molecular probe. Osteoclast proton pumps, which are vacuolar H^+-ATPases (V-type H^+-ATPases), are majorly involved in the secretion of several protons to dissolve bone minerals.[19] Mutation in proton pumps disrupts osteoclast activity and leads to osteopetrosis.[20] They comprise multiple subunits, and the *a*3 isoform of the *a* subunit is suitable as a marker for mature osteoclasts. A recent study reported the distinct localization and motility of osteoclast proton pumps in fluorescent reporter mice, where green fluorescent protein (GFP) is expressed under the promoter of the V-type H^+-ATPase *a*3 subunit (*a*3-GFP mice).[21,22] However, the mechanism by which mature osteoclasts regulate the localization of the proton pumps upon bone resorption is still unclear due to the lack of spatiotemporal information on acidic compartments. To address this issue, it is necessary to simultaneously visualize the GFP-labeled proton pumps and acidic compartments with different fluorescence colors. Thus far, various pH-activatable fluorophores have been developed and employed to detect extracellular and intracellular pH;[23,24] however, they have not yet been applied for imaging the *in vivo* dynamics of proton pumps. Thus, we developed a novel red fluorescent small-molecular probe, Red-pHocas, with rapid reversible pH-sensing and bone-targeting properties, for multicolor imaging of acidic compartments and the analysis of osteoclast proton pump dynamics in living mice (Figure 1). We designed a series of rhodamine spirolactams and rationally controlled the fluorescence response kinetics in acidic pH conditions by the introduction of *N*-alkyl groups in the spirolactam. As a result, acceleration of the fluorescence response in Red-pHocas aided the visualization of the acidic compartments in the bone tissue with a high temporal resolution, which enabled a detailed imaging analysis of the dynamics of osteoclast proton pumps in *a*3-GFP-mice. The spatiotemporal analysis between subcellular distributions of the osteoclast proton pumps and the acidic compartments revealed the functional correlations of osteoclast proton pumps with bone resorption *in vivo*.

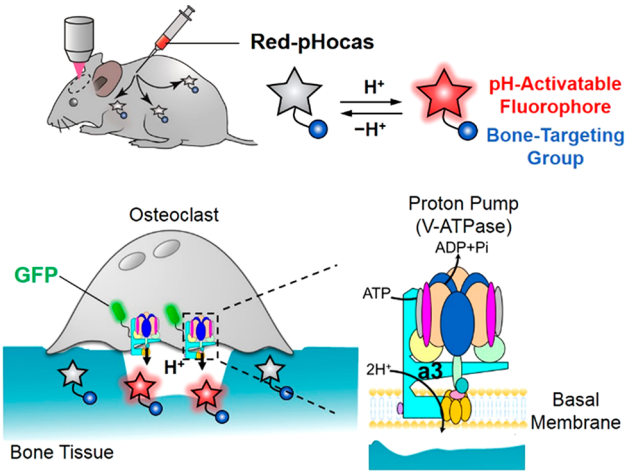

Figure 1. Schematic illustration of a multicolor intravital imaging system for osteoclast proton pump dynamics and function with Red-pHocas (a pH-activatable red fluorescent probe) in *a*3-GFP mice.

RESULTS

Design Synthesis and Evaluation of pH-Activatable Fluorescent Dyes Based on Rhodamine Spirolactams. We designed a novel red fluorescent probe for imaging the acidic regions created by activated osteoclasts *in vivo* (Figure 2a). Rhodamine was selected as a fluorophore moiety of the probe due to its high photostability and the compatibility of multicolor imaging with GFP-expressing reporter mice. In addition, rhodamines have broad two-photon excitation spectra in the range 780−1000 nm,[25] where other fluorescent proteins can be excited simultaneously. Bisphosphonate groups are introduced to improve the aqueous solubility of hydrophobic rhodamine dyes and strengthen their affinity for bone tissues, allowing biocompatibility and efficient delivery of the dyes by adsorption onto bone tissues.[14,15] The pH-activatable property is afforded by a reversible spirocyclization reaction in rhodamine spirolactams. The fluorescence activation corresponds to the regulation of the spirocyclization reaction between a closed nonfluorescent and colorless form at higher pHs and an open fluorescent form in lower pHs. Such pH-activatable rhodamine spirolactams have been developed previously.[26−30]

Thus, we initially synthesized and evaluated pH-activatable fluorescence properties of a series of rhodamine spirolactams Rh-1−3 based on a rhodamine-B dye (Figure 2b and Scheme S1). Rh-2 with an electron-withdrawing group (2,2,2-trifluoroethyl) and Rh-3 with a bulky group (cyclohexyl) were designed to investigate the effect of the spirocyclization reaction on the electronic and steric factors in the *N*-alkyl substituents of the spirolactams, respectively. For further conjugation of bisphosphonates, two carboxylic acids were introduced into the dyes.

The fluorescence spectra of Rh-1−3 were measured at different pH regions (Figure S1). All rhodamine derivatives showed a fluorescence increase at the lowered pH regions and distinct pH profiles depending on the structures (Figure 2c). The pK_a values of Rh-1−3 ranged from 4.9 to 5.9 (Figure 2c and Table S1), which is suitable for imaging acidic areas created by mature osteoclasts.[14]

Among Rh-1−3, the pK_a of Rh-3 (5.9) that had a sterically bulky cyclohexyl group was higher than that of Rh-1 (4.9), which had a smaller ethyl substituent, indicating the dependency of pK_a on the size of the *N*-alkyl substituents in the spirolactams.

Furthermore, the ring-opening reactions of the spirolactam were monitored by assessing the absorption transition of the dyes upon an immediate pH jump from pH 8.0 to 4.0 achieved by exchanging the buffer (Figure 2d). In the rhodamine spirolactams, the kinetics of the ring-opening reaction reflect the fluorescence response rate following the change to acidic pH.

DOI: 10.1021/acscentsci.9b00220
ACS Cent. Sci. 2019, 5, 1059−1066

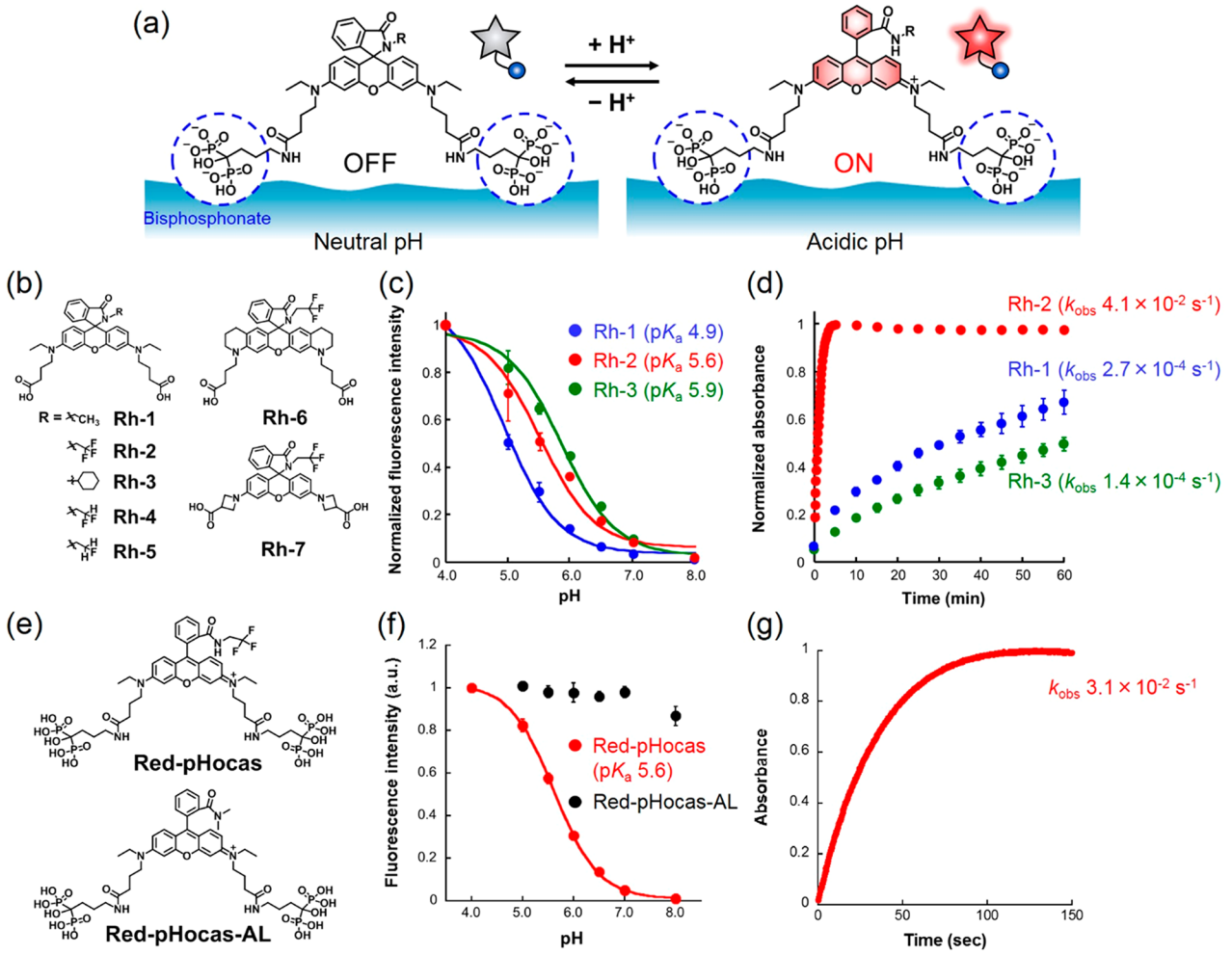

Figure 2. Development of Red-pHocas for detecting bone-resorbing compartments. (a) Design of Red pH-activatable fluorescent probe (Red-pHocas) for detecting the acidic region in bone tissues. (b) Chemical structures of rhodamine spirolactam-based dyes Rh-1−7. (c) pH profile of fluorescence intensity of Rh-1−3 (0.2 μM) in 0.1 M citrate-phosphate buffer at 37 °C. Excited at 535 nm. (d) Time-course absorbance of Rh-1−3 (10 μM) at maximum absorption wavelengths upon a pH jump from 8.0 to 4.0 at 37 °C. (e) Chemical structures of Red-pHocas (pH-activatable) and Red-pHocas-AL (always-ON-type). (f) pH profile of the fluorescence intensity of Red-pHocas and Red-pHocas-AL (0.2 μM) in 0.1 M citrate-phosphate buffer at 37 °C. Excited at 535 nm. (g) Time-course absorbance at 562 nm of Red-pHocas (10 μM) upon a pH jump from 8.0 to 4.0 at 37 °C. Error bars represent standard deviation (N = 3).

Remarkably, Rh-2 quickly reached steady absorbance with an apparent rate constant (k_{obs}) of 4.1 × 10^{-2} s^{-1} after the acidification of the solution, whereas the absorbance peaks of Rh-1 and Rh-3 continued to increase even after 60 min (k_{obs} = 2.7 × 10^{-4} s^{-1} for Rh-1 and 1.4 × 10^{-4} s^{-1} for Rh-3, Table S1). This result indicates that an electron-withdrawing 2,2,2-trifluoroethyl group contributes to a rapid ring-opening reaction upon protonation. The difference in the reaction rate can be explained by the electronic effect of the *N*-alkyl substituents on the stability of the protonated rhodamine spirolactam. Electron-withdrawing substituents destabilize the protonated intermediate, resulting in a rapid ring-opening reaction to form the fluorescent structure (Figure S5). To examine the rate enhancement of fluorescence activation by the electron-withdrawing group, the fluorescence activation responses were further evaluated in the rhodamine spirolactams substituted with 2-di- and monofluorinated ethyl groups (Rh-4 and Rh-5 in Figure 2b). The results revealed that the response rate constants increased with the increase in the number of fluorine atoms in the *N*-alkyl substituents (k_{obs} = 4.6 × 10^{-3} s^{-1} for Rh-4 and 1.4 × 10^{-3} s^{-1} for Rh-5, Figure S4a and Table S1). Moreover, we confirmed that trifluoroethyl-modified rhodamine spirolactams show rapid fluorescence activation in other rhodamine scaffolds like a bis(tetrahydroquinoline)- and a bis(azetidinyl)-rhodamine, which possess different pK_a values (Rh-6 and Rh-7 in Figure 2b and Figures S3b and S4b), indicating the versatility of this strategy in increasing the fluorescence response kinetics based on the spirocyclization reaction. The fluorescence intensities of the dyes at acidic pH were evaluated by comparing those in 0.1% (SDS) that induces fully opened structures (Figure S6). Because of the suitable pK_a and the rapid fluorescence activation response, Rh-2 was selected as a dye structure for detecting the area of bone acidification *in vivo*.

Development of Red-pHocas for Detecting Bone-Resorbing Compartments. Furthermore, we synthesized a small-molecular probe Red-pHocas by the conjugation of Rh-2 with two alendronates containing bone-targeting bisphosphonate groups (Figure 2e and Scheme S5). The pH response curve and the activation response rate of Red-pHocas were similar to those of the parent fluorophore Rh-2 (Figure 2f,g and Table S2), indicating that the introduction of the bisphosphonates retains the fluorescence properties of the rhodamine spirolactam dye.

DOI: 10.1021/acscentsci.9b00220
ACS Cent. Sci. 2019, 5, 1059−1066

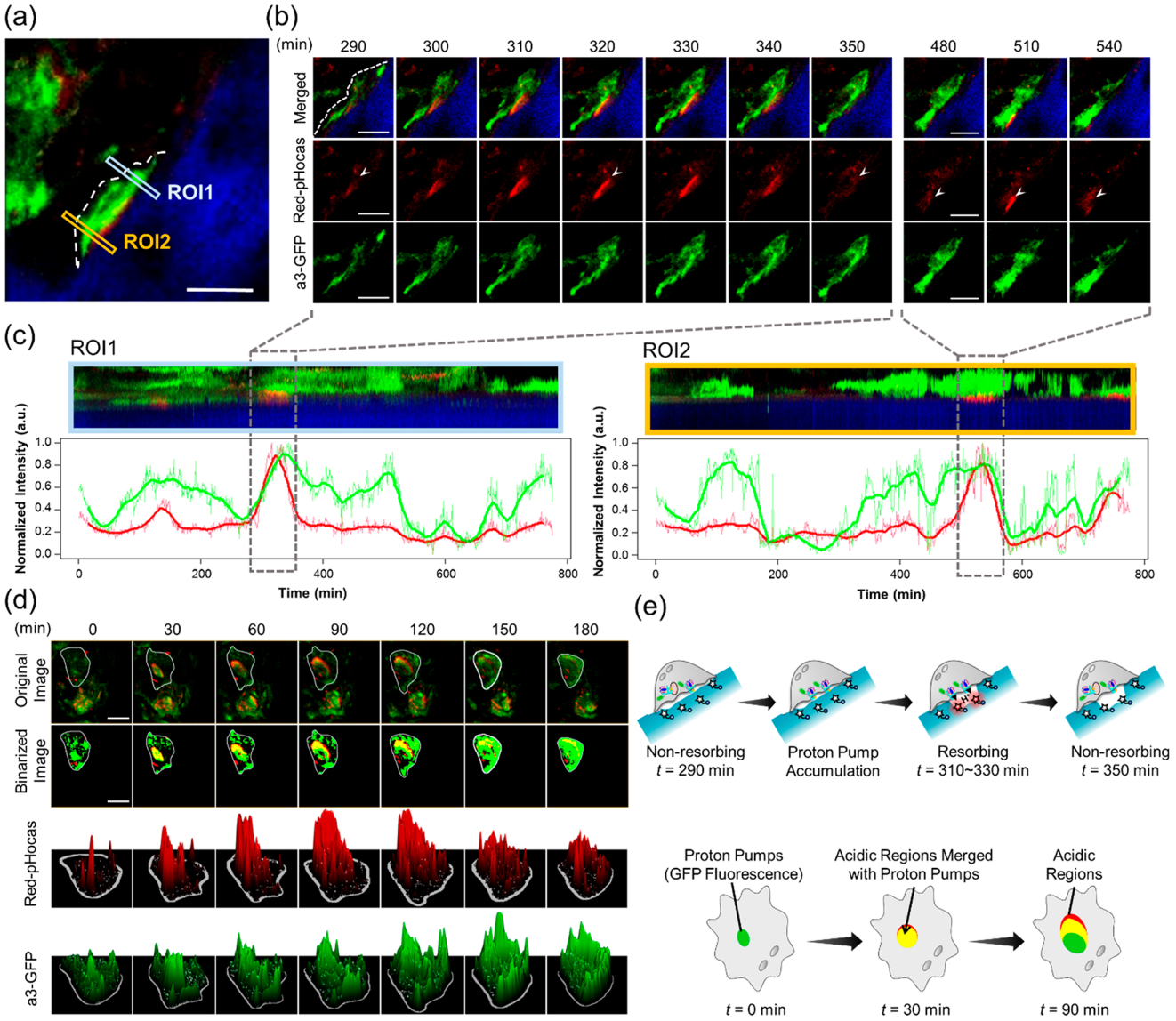

Figure 3. Correlation analysis of osteoclast proton pumps and acidic regions on the bone surface. (a) Intravital two-photon fluorescence imaging of bone tissue after injection of Red-pHocas at the interval of 1 min. Squares indicate the region of interest (ROI). (b) Time-lapse two-photon fluorescence imaging of osteoclasts in bone tissues captured at 290−350 and 480−540 min. A white dash line and arrowheads indicate cell border and acidic regions, respectively. (c) Kymographs of fluorescence intensity of Red-pHocas (red) and *a*3-GFP (green) in ROI 1 (left) and ROI 2 (right) of part a. Each kymograph corresponds to the area marked by a rectangle in part a. The vertical axis corresponds the direction from the bone tissue to the cavity, and the horizontal axis indicates a lapse of time. The line charts under the kymographs present the mean intensities of Red-pHocas and *a*3-GFP (each bold line is the time-smoothed mean intensity by using the moving average). (d) Time-lapse two-photon fluorescence images of osteoclasts captured at 0−180 min. Original images, binarized images, and 3D surface plots of Red-pHocas and *a*3-GFP are shown from the top. In 3D surface plots, fluorescence intensities were indicated as heights. White lines indicate cell borders. (e) Schematic illustrations of proton pump dynamics and acidic regions in osteoclasts in parts b (top) and d (bottom), respectively. Dose: 10 mg/kg (3 days). Excited at 860 nm. Scale bars: 20 μm. Green, GFP-fused proton pumps; red, Red-pHocas; blue, bone tissue; yellow, acidic regions merged with proton pumps.

The effects on pK_a and activation rate are limited, since the conjugation of bisphosphonates possibly does not affect the steric/electronic properties of *N*-alkyl substituents of the lactam or the electronic properties of xanthene rings that are associated with the spirocyclization reaction.[29] The reversibility of pH sensing in Red-pHocas was confirmed by repetitive pH variation from neutral to acidic buffer (Figure S7). Red-pHocas revealed negligible photobleaching after continuous irradiation with the excitation light, which is comparable to the green fluorescent probe in our previous study (Figure S8).[15] The pH-dependent fluorescence property of Red-pHocas was also considered after adsorption on hydroxyapatite (HA) particles, a model substrate of bone tissue (Figure S9). These results indicate the imaging capability of acidic regions in bone tissue during a long period of time.

As a control fluorescent probe, always-ON-type, Red-pHocas-AL, was synthesized by introducing a secondary *N*,*N*-dimethyl amide to prevent the spirocyclization-mediated fluorescence quenching (Figure 2e and Schemes S2 and S5). The fluorescence intensity of Red-pHocas-AL was constant in pH regions at 4.0−8.0 in solution and when adsorbed on HA (Figure 2f and Figure S9). The adsorbed probes were not detached even in the presence of excess amount of alendronates

DOI: 10.1021/acscentsci.9b00220
ACS Cent. Sci. 2019, 5, 1059−1066

(Figure S10), indicating irreversible binding to the hydroxyapatite, the major bone mineral, once they attached.

Multicolor Intravital Imaging of Osteoclast Proton Pumps and Acidic Regions on the Bone Surface. Next, we examined whether Red-pHocas can detect acidic regions created by activated osteoclasts in the bone tissues in living mice. Red-pHocas or always-ON-type probe Red-pHocas-AL was administrated subcutaneously to *a*3-GFP knock-in mice for 3 days. The bone volume was not changed after the treatment with Red-pHocas under the same conditions for intravital imaging (Figure S11), which suggests that bone metabolism is hardly affected by treatment with the probe.

To confirm the distribution and the pH-activatable property of Red-pHocas, we performed fluorescence imaging of the fixed bone tissue section from a mouse after the probe administration (Figure S12). The fluorescence signals of Red-pHocas were detected along the bone surface in a pH-dependent manner, indicating the delivery activity of the pH-activatable probe to the bone surface.

Moreover, we performed intravital imaging of calvaria bone tissue in the probe-administrated mice using two-photon excitation microscopy under anesthesia. Considering the spectral overlap of the two-photon excitation of Red-pHocas and GFP (Figure S13), we determined 860 nm as a suitable excitation wavelength to simultaneously excite the fluorophores.

Fluorescence images were acquired after processing the spectral unmixing algorithms that separate distinct fluorescence signals derived from GFP, Red-pHocas (or Red-pHocas-AL), and second-harmonic generation (SHG) of collagen fibers in bones. The fluorescence signals of osteoclast proton pumps were distributed along the osteoclastic plasma membranes, as confirmed in crossing *a*3-GFP mice with reporter ones expressing tdTomato (a red fluorescent protein) under the promoter of the tartrate-resistant acid phosphatase (TRAP) as a marker of mature osteoclasts (Figure S14). We also found that the fluorescence signals of Red-pHocas in the local area on the bone surface overlapped with osteoclast localizations (Figure 3a).

Conversely, the fluorescence signals of Red-pHocas-AL were distributed over the bone surface (Figure S15). These results indicate that both fluorescent probes were delivered to the bone surfaces, and Red-pHocas selectively detected the lowered pH regions upon bone resorption by activated osteoclasts. The fluorescence signals of Red-pHocas remained steady during 60 min of observation (Movie S1), indicating the sufficient photostability of the rhodamine-based dyes for longitudinal *in vivo* imaging.

Correlation Analysis between Osteoclast Proton Pumps and Acidic Regions on the Bone Surface. To investigate the correlation between the dynamics of osteoclast proton pumps and bone acidification, time-lapse imaging with Red-pHocas was performed in bone tissues in an *a*3-GFP mouse. The dynamics of osteoclast proton pumps with the acidic compartments were simultaneously monitored over a long time. In an osteoclast on the bone surface from a lateral view, time-lapse imaging revealed the localization changes of the osteoclast proton pump and fluctuations of the acidic regions at the osteoclast-adsorbed bone surface (Figure 3b and Movie S2). We found that the osteoclast proton pumps were sparsely distributed at the membrane and intracellular compartments in the osteoclast where few acidic regions were detected (t = 290 min). Concomitant with the accumulation of the osteoclast proton pumps on the bone surface, the acidic compartments emerged and spread over the bone surface covered by the osteoclast (t = 310−330 min). Thereafter, the area of acidic compartments on the bone surface was gradually decreased (t = 350 min) without the localization change of the osteoclast proton pumps, indicating that the osteoclast was in an inactive, nonresorbing state.

Moreover, we also measured the spatiotemporal fluctuation of the acidic regions and the proton pump accumulation using kymograph analysis in two regions (ROI 1 and ROI 2 in Figure 3c). From the red fluorescence signal intensities, the time periods of bone acidification by this osteoclast were approximately 1 h in ROI 1 and ROI 2. In addition, the enhanced red fluorescence signals were detected with green fluorescence signals, indicating that bone acidification was associated with proton pump accumulation to the bone surface (Figure 3e).

In a top view of the osteoclast on the bone surface, we observed the partial overlap of acidic regions with the regions containing the proton pumps at the leading edge of osteoclast cell membranes (Figure 3d and Movie S3). Moreover, the acidic regions were persistently migrating from the center to the periphery of the osteoclasts along with a change in the proton pump localizations (t = 0−180 min). Such dynamics of a resorptive osteoclast were found in the bone tissue in living mice.[15] From 3D surface plots and binarized images, the sizes of acidic regions and the proton pumps were gradually increased (Figure 3d), indicating the expansion of the area of bone acidification with the spread of the proton pumps in the osteoclast. The intensity of the red fluorescence signals was fluctuated, suggesting the local pH variation. These results revealed the strong correlation between the localizations of the osteoclast proton pumps and acidic regions upon bone resorption.

Quantitative Analysis of Function of Osteoclast Proton Pumps upon Drug Response. We applied our imaging system to the *in vivo* quantitative evaluation of drugs targeting osteoclast proton pumps. Bafilomycin A1 is a known proton pump inhibitor that binds to proton pumps to inhibit the proton transport by preventing the rotation of the proteolipid c-ring;[31,32] however, the effects on *in vivo* dynamics of osteoclast proton pumps have not been examined. Furthermore, bafilomycin A1 was intravenously injected to *a*3-GFP mice treated with Red-pHocas during imaging experiments. We found that the red fluorescent signals gradually decreased in the whole area of view (Figure 4a). Statistical analysis of the acidic regions overlapping with proton pumps revealed a significant reduction by 70% and 52% after 30 and 60 min of treatment with bafilomycin A1, respectively (Figure 4b).

In contrast, treatment with the vehicle did not change the fluorescence intensity significantly (Figure 4c,d). On the other hand, the localizations of osteoclast *a*3-GFP proton pumps were not significantly changed after treatment with bafilomycin A1, indicating that inhibition of the proton pump function does not affect its subcellular distribution and motility. We newly found the action of drugs in terms of the dynamics and function by simultaneous imaging of the localizations of osteoclast proton pumps and acidic regions *in vivo*.

Safety Statement. No unexpected or unusually high safety hazards were encountered.

DISCUSSION

We developed the Red-pHocas that enabled the imaging of the fluctuating lowered pH regions in osteoclast basal membranes to reveal the function of osteoclast proton pumps. Red-pHocas

DOI: 10.1021/acscentsci.9b00220
ACS Cent. Sci. 2019, 5, 1059−1066

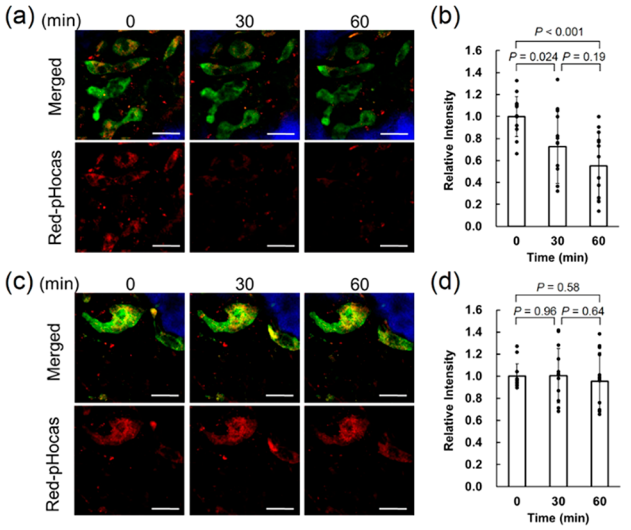

Figure 4. Quantitative analysis of the function of osteoclast proton pumps upon drug response. (a) Intravital two-photon fluorescence imaging of the function of osteoclast proton pumps treated with bafilomycin A1 (0.5 mg/kg). (b) Changes in fluorescence intensity normalized to the initial intensity after treatment with bafilomycin A1. (c) Intravital two-photon fluorescence imaging of the function of osteoclast proton pumps treated with the vehicle. (d) Changes in the fluorescence intensity after treatment with the vehicle. Excited at 860 nm. Scale bars: 30 μm. Error bars represent averages ± SD (N = 13 collected from 3 independent experiments, respectively). Green, GFP-fused proton pumps; red, Red-pHocas; blue, bone tissue.

possesses a bone-targeting ability and reversible pH-activatable property with quick response based on a photostable rhodamine scaffold (Figure 2f,g); these are suitable for the longitudinal monitoring of lowered pH regions and the proton pump dynamics within these regions in bone tissues. To date, several rhodamine-based pH-activatable probes have been developed;[26−30,33−35] however, the relationship between their structures and fluorescence properties has not been sufficiently discussed. Hence, it is challenging to design fluorescent probes with a desired pH sensitivity and response kinetics for targeted biological applications. In this study, we have provided probe design guidelines to control fluorescence activation responses by simply modifying *N*-alkyl substituents in rhodamine spirolactams. In particular, introduction of the 2,2,2-trifluoroethyl group into the *N*-alkyl amide substituent (Rh-2) significantly enhanced the response time of the fluorescence activation (Figure 2d). In rhodamine spirolactams, the fluorescence activation proceeds via protonation on the lactam amide, followed by the opening of the spirolactam ring (Figure S5).[29,30] As the second step can be considered a rate-limiting step, the various responses are attributed to the stability of the protonated intermediates in ring-closed structures. Therefore, the enhanced fluorescence turn-on response in Rh-2 can be explained by the destabilization of the intermediates caused by the electron-withdrawing effects of the 2,2,2-trifluoroethyl group. Using these design guidelines, the kinetics of the fluorescence activation were rationally controlled in rhodamine spirolactams (Figure 2d and Figure S4a). The reversible quick pH-response property of Red-pHocas allowed the long-term multicolor imaging of acidic regions and proton pump dynamics with a high temporal resolution by simultaneous two-photon excitation of the fluorophores (Movies S2 and S3).

We also found that the pK_a values were dependent on the size of the *N*-alkyl substituents in the rhodamine-B-based fluorophores Rh-1−3 (Figure 2c), suggesting that bulky *N*-substituents at the spirolactam can destabilize the non-fluorescent ring-closed structure.[28] In contrast, the pH-responsive property can be substantially modulated without decreasing the response kinetics by use of different rhodamine scaffolds; the 2,2,2-trifluoroethyl group was introduced into the spirolactam amides of these scaffolds (Figures S3b and S4b). Although these fluorophores indicated considerable pK_a shifts beyond the range for sensing osteoclast activity, they can be employed to rapidly detect pH variations in more acidic or neutral regions. By altering active targeting moieties such as small-molecular ligands and antibodies, the local pH around target biomolecules can be imaged *in vivo*. It is difficult to visualize the actual pH in bone tissue using the current imaging system. Combining injectable pH-activatable green/red fluorescent probes with different pH responses, detailed pH mapping at bone surfaces can be obtained, and the actual pH can be quantified by ratiometric analysis.

During osteoclast differentiation, the ATP-driven proton pumps are translocated from intracellular vesicles to ruffled border membranes, implying the involvement of the proton pump localization with bone resorption.[36−40] The polar distribution of osteoclast proton pumps in the basal membrane was observed by immunohistochemical analysis. Nevertheless, the requirement of cell fixation impairs the dynamics of proton pumps and the function of proton secretion. Hence, the correlation of the localizations of osteoclast proton pumps with acidic regions in living animals has not been clarified. In contrast, the intravital imaging system provides information on *in vivo* dynamics of the proton pumps with a subcellular resolution without fixation of tissue samples. We found that the proton pumps dynamically migrate in the osteoclast and accumulate along the basal membranes in bone resorption (Figure 3c). Moreover, using a functional chemical probe, we observed the spatial overlap of the acidic regions and osteoclast proton pump distributions (Figure 3b,d and Movies S2 and S3) and the synchronous proton secretion with proton pump accumulation (Figure 3c). These results were the first to demonstrate the direct involvement of the proton pumps in bone acidification in living animals. In addition, the drug response of osteoclast bone resorption activity and proton pump motility was quantitatively evaluated in a time-dependent manner (Figure 4). Recent results reveal that osteoclast activity is involved in a broad range of bone diseases such as rheumatoid arthritis and metastatic bone cancer.[41,42] Antiresorptive bisphosphonates act differently *in vivo* depending on their bone binding affinities and farnesyl pyrophosphate synthase inhibitory activities.[43] Furthermore, it has been reported that trafficking defects in proton pumps inhibit proton secretion from osteoclasts.[44] Our imaging approach can spatiotemporally analyze the drug efficacies in intact tissues and provide a useful tool for the development of drugs against bone diseases and inhibitors of trafficking pathways of proton pumps.

CONCLUSION

In conclusion, we developed a red fluorescent pH-activatable probe, Red-pHocas, for monitoring the acidic environment in bone tissue *in vivo*. The increase of pH-response kinetics in the rhodamine spirolactams enables the imaging of pH fluctuations in bone surfaces with a high temporal resolution, which reveal the dynamics and function of osteoclast proton pumps by

DOI: 10.1021/acscentsci.9b00220
ACS Cent. Sci. 2019, 5, 1059−1066

multicolor imaging. Multicolor intravital imaging via functional fluorescent probes will be a powerful tool for the spatiotemporal analysis of the dynamics and function of biomolecules, which can elucidate their physiological function in living animals at a molecular level.

■ ASSOCIATED CONTENT

Supporting Information

The Supporting Information is available free of charge on the ACS Publications website at DOI: 10.1021/acscentsci.9b00220.

Materials and methods, synthetic procedures and characterization of compounds, detailed experimental procedures, absorbance and fluorescence spectroscopic data, fluorescence images, analysis of the bone volume fraction, two-photon excitation spectra, and two-photon fluorescence images (PDF)

Movie S1: two-photon time-lapse imaging of bone tissue after injection of Red-pHocas-AL at an interval of 1 min for 60 min (MPG)

Movie S2: two-photon time-lapse imaging of bone tissue after injection of Red-pHocas with spectral unmixing at an interval of 1 min for 270 min (MPG)

Movie S3: two-photon time-lapse imaging of bone tissue after injection of Red-pHocas with spectral unmixing at an interval of 5 min for 3 h (MPG)

■ AUTHOR INFORMATION

Corresponding Author

*E-mail: kkikuchi@mls.eng.osaka-u.ac.jp.

ORCID

Kazuya Kikuchi: 0000-0001-7103-1275

Funding

This research was supported by the Grant-in-Aid for Scientific Research (Grant 16K01933 to M. Minoshima, 15H056710 to J. Kikuta, 16H026190 to M. Ishii, 25220207, 18H03935 to K. Kikuchi), Innovative Areas "Frontier Research on Chemical Communications" (17H06409) of Ministry of Education, Culture, Sports, Science, and Technology (MEXT) of Japan; CREST, the Japan Science and Technology Agency (170701506 to M. Ishii); PRIME from Japan Agency for Medical Research and Development (AMED, JP18gm6210005 to J. Kikuta); AMED (18he0902005h0004, 17ae0101041h9902, 18fm0208018h0002 to K. Kikuchi); JSPS A3 Foresight Program; and JSPS CORE-to-CORE Program "Asian Chemical Biology Initiative".

Notes

The authors declare no competing financial interest.

■ ACKNOWLEDGMENTS

The authors would like to thank Prof. Takashi Hayashi and Dr. Koji Oohora (Graduate School of Engineering, Osaka University) for the experiment using a stopped-flow absorption spectrometer.

■ REFERENCES

(1) Helmchen, F.; Denk, W. Deep tissue two-photon microscopy. *Nat. Methods* **2005**, *2*, 932−940.

(2) Miller, M. J.; Wei, S. H.; Parker, I.; Cahalan, M. D. Two-photon imaging of lymphocyte motility and antigen response in intact lymph node. *Science* **2002**, *296*, 1869−1873.

(3) Stroh, M.; Zimmer, J. P.; Duda, D. G.; Levchenko, T. S.; Cohen, K. S.; Brown, E. B.; Scadden, D. T.; Torchilin, V. P.; Bawendi, M. G.; Fukumura, D.; Jain, R. K. Quantum dots spectrally distinguish multiple species within the tumor milieu *in vivo*. *Nat. Med.* **2005**, *11*, 678−682.

(4) Kedrin, D.; Gligorijevic, B.; Wyckoff, J.; Verkhusha, V. V.; Condeelis, J.; Segall, J. E.; Van Rheenen, J. Intravital imaging of metastatic behavior through a mammary imaging window. *Nat. Methods* **2008**, *5*, 1019−1021.

(5) Giampieri, S.; Manning, C.; Hooper, S.; Hill, C. S.; Sahai, E. Localized and reversible TGF signalling switches breast cancer cells from cohesive to single cell motility. *Nat. Cell Biol.* **2009**, *11*, 1287−1296.

(6) Ishii, M.; Egen, J. G.; Klauschen, F.; Meier-Schellersheim, M.; Saeki, Y.; Vacher, J.; Proia, R. L.; Germain, R. N. Sphingosine-1-phosphate mobilizes osteoclast precursors and regulates bone homeostasis. *Nature* **2009**, *458*, 524−528.

(7) Bousso, P.; Bhakta, N. R.; Lewis, R. S.; Robey, E. Dynamics of thymocyte-stromal cell interactions visualized by two-photon microscopy. *Science* **2002**, *296*, 1876−1880.

(8) Stoll, S.; Delon, J.; Brotz, T. M.; Germain, R. N. Dynamic imaging of T cell-dendritic cell interactions in lymph nodes. *Science* **2002**, *296*, 1873−1876.

(9) Furuya, M.; Kikuta, J.; Fujimoto, S.; Seno, S.; Maeda, H.; Shirazaki, M.; Uenaka, M.; Mizuno, H.; Iwamoto, Y.; Morimoto, A.; Hashimoto, K.; Ito, T.; Isogai, Y.; Kashii, M.; Kaito, T.; Ohba, S.; Chung, U.; Lichtler, A. C.; Kikuchi, K.; Matsuda, H.; Yoshikawa, H.; Ishii, M. Direct cell-cell contact between mature osteoblasts and osteoclasts dynamically controls their functions in vivo. *Nat. Commun.* **2018**, *9*, 300.

(10) Miller, M. A.; Weissleder, R. Imaging of anticancer drug action in single cells. *Nat. Rev. Cancer* **2017**, *17*, 399.

(11) Hirata, E.; Girotti, M. R.; Viros, A.; Hooper, S.; Spencer-Dene, B.; Matsuda, M.; Larkin, J.; Marais, R.; Sahai, E. Intravital imaging reveals how BRAF inhibition generates drug-tolerant microenvironments with high integrin β1/FAK signaling. *Cancer Cell* **2015**, *27*, 574−588.

(12) Breart, B.; Lemaître, F.; Celli, S.; Bousso, P. Two-photon imaging of intratumoral $CD8^+$ T cell cytotoxic activity during adoptive T cell therapy in mice. *J. Clin. Invest.* **2008**, *118*, 1390−1397.

(13) Lavis, L. D.; Raines, R. T. Bright ideas for chemical biology. *ACS Chem. Biol.* **2008**, *3*, 142−155.

(14) Kowada, T.; Kikuta, J.; Kubo, A.; Ishii, M.; Maeda, H.; Mizukami, S.; Kikuchi, K. *In vivo* fluorescence imaging of bone-resorbing osteoclasts. *J. Am. Chem. Soc.* **2011**, *133*, 17772−17776.

(15) Maeda, H.; Kowada, T.; Kikuta, J.; Furuya, M.; Shirazaki, M.; Mizukami, S.; Ishii, M.; Kikuchi, K. Real-time intravital imaging of pH variation associated with osteoclast activity. *Nat. Chem. Biol.* **2016**, *12*, 579−585.

(16) Teitelbaum, S. L. Bone resorption by osteoclasts. *Science* **2000**, *289*, 1504−1508.

(17) Boyle, W. J.; Simonet, W. S.; Lacey, D. L. Osteoclast differentiation and activation. *Nature* **2003**, *423*, 337−342.

(18) Kozloff, K. M.; Quinti, L.; Patntirapong, S.; Hauschka, P. V.; Tung, C. H.; Weissleder, R.; Mahmood, U. Non-invasive optical detection of cathepsin K-mediated fluorescence reveals osteoclast activity *in vitro* and *in vivo*. *Bone.* **2009**, *44*, 190−198.

(19) Marshansky, V.; Futai, M. The V-type H^+-ATPase in vesicular trafficking: targeting, regulation and function. *Curr. Opin. Cell Biol.* **2008**, *20*, 415−426.

(20) Frattini, A.; Orchard, P. J.; Sobacchi, C.; Giliani, S.; Abinun, M.; Mattsson, J. P.; Keeling, D. J.; Andersson, A.-K.; Wallbrandt, P.; Zecca, L.; Notarangelo, L. D.; Vezzoni, P.; Villa, A. Defects in TCIRG1 subunit of the vacuolar proton pump are responsible for a subset of human autosomal recessive osteopetrosis. *Nat. Genet.* **2000**, *25*, 343−346.

(21) Sun-Wada, G. H.; Tabata, H.; Kawamura, N.; Aoyama, M.; Wada, Y. Direct recruitment of H^+-ATPase from lysosomes for phagosomal acidification. *J. Cell Sci.* **2009**, *122*, 2504−2513.

(22) Kikuta, J.; Wada, Y.; Kowada, T.; Wang, Z.; Sun-Wada, G. H.; Nishiyama, I.; Mizukami, S.; Maiya, N.; Yasuda, H.; Kumanogoh, A.; Kikuchi, K.; Germain, R. N.; Ishii, M. Dynamic visualization of RANKL

and Th17-mediated osteoclast function. *J. Clin. Invest.* **2013**, *123*, 866−873.
(23) Han, J.; Burgess, K. Fluorescent indicators for intracellular pH. *Chem. Rev.* **2010**, *110*, 2709−2728.
(24) Yin, J.; Hu, Y.; Yoon, J. Fluorescent probes and bioimaging: alkali metals, alkaline earth metals and pH. *Chem. Soc. Rev.* **2015**, *44*, 4619−4644.
(25) Mütze, J.; Iyer, V.; Macklin, J. J.; Colonell, J.; Karsh, B.; Petrášek, Z.; Schwille, P.; Looger, L. L.; Lavis, L. D.; Harris, T. D. Excitation spectra and brightness optimization of two-photon excited probes. *Biophys. J.* **2012**, *102*, 934−944.
(26) Zhang, W.; Tang, B.; Liu, X.; Liu, Y.; Xu, K.; Ma, J.; Tonga, L.; Yang, G. A highly sensitive acidic pH fluorescent probe and its application to HepG2 cells. *Analyst* **2009**, *134*, 367−371.
(27) Li, Z.; Wu, S.; Han, J.; Han, S. Imaging of intracellular acidic compartments with a sensitive rhodamine based fluorogenic pH sensor. *Analyst* **2011**, *136*, 3698−3706.
(28) Yuan, L.; Lin, W.; Feng, Y. A rational approach to tuning the pK_a values of rhodamines for living cell fluorescence imaging. *Org. Biomol. Chem.* **2011**, *9*, 1723−1726.
(29) Montenegro, H.; Di Paolo, M.; Capdevila, D.; Aramendía, P. F.; Bossi, M. L. The mechanism of the photochromic transformation of spirorhodamines. *Photochem. Photobiol. Sci.* **2012**, *11*, 1081−1086.
(30) Czaplyski, W. L.; Purnell, G. E.; Roberts, C. A.; Allred, R. M.; Harbron, E. J. Substituent effects on the turn-on kinetics of rhodamine-based fluorescent pH probes. *Org. Biomol. Chem.* **2014**, *12*, 526−533.
(31) Bowman, E. J.; Siebers, A.; Altendorf, K. Bafilomycins: a class of inhibitors of membrane ATPases from microorganisms, animal cells, and plant cells. *Proc. Natl. Acad. Sci. U. S. A.* **1988**, *85*, 7972−7976.
(32) Bowman, B. J.; McCall, M. E.; Baertsch, R.; Bowman, E. J. A model for the proteolipid ring and bafilomycin/concanamycin binding site in the vacuolar ATPase of *Neurosporacrassa. J. Biol. Chem.* **2006**, *281*, 31885−31893.
(33) Best, Q. A.; Xu, R.; McCarroll, M. E.; Wang, L.; Dyer, D. J. Design and investigation of a series of rhodamine-based fluorescent probes for optical measurements of pH. *Org. Lett.* **2010**, *12*, 3219−3221.
(34) Bender, A.; Woydziak, Z. R.; Fu, F.; Branden, M.; Zhou, Z.; Ackley, B. D.; Peterson, B. R. Novel acid-activated fluorophores reveal a dynamic wave of protons in the intestine of *Caenorhabditis elegans. ACS Chem. Biol.* **2013**, *8*, 636−642.
(35) Liu, C.; Best, Q. A.; Suarez, B.; Pertile, J.; McCarroll, M. E.; Scott, C. N. Cycloalkyl-aminomethylrhodamines: pH dependent photophysical properties tuned by cycloalkane ring size. *J. Fluoresc.* **2015**, *25*, 231−237.
(36) Blair, H. C.; Teitelbaum, S. L.; Ghiselli, R.; Gluck, S. Osteoclastic bone resorption by a polarized vacuolar proton pump. *Science* **1989**, *245*, 855−857.
(37) Nakamura, H.; Moriyama, Y.; Futai, M.; Ozawa, H. Immunohistochemical localization of vacuolar H^+-ATPase in osteoclasts of rat tibiae. *Arch. Histol. Cytol.* **1994**, *57*, 535−539.
(38) Väänänen, H. K.; Karhukorpi, E. K.; Sundquist, K.; Wallmark, B.; Roininen, I.; Hentunen, T.; Tuukkanen, J.; Lakkakorpi, P. Evidence for the presence of a proton pump of the vacuolar H (+)-ATPase type in the ruffled borders of osteoclasts. *J. Cell Biol.* **1990**, *111*, 1305−1311.
(39) Toyomura, T.; Oka, T.; Yamaguchi, C.; Wada, Y.; Futai, M. Three subunit *a* isoforms of mouse vacuolar H^+-ATPase preferential expression of the *a*3 isoform during osteoclast differentiation. *J. Biol. Chem.* **2000**, *275*, 8760−8765.
(40) Toyomura, T.; Murata, Y.; Yamamoto, A.; Oka, T.; Sun-Wada, G. H.; Wada, Y.; Futai, M. From lysosomes to the plasma membrane localization of vacuolar type H^+-ATPase with the *a*3 isoform during osteoclast differentiation. *J. Biol. Chem.* **2003**, *278*, 22023−22030.
(41) Matsuura, Y.; Kikuta, J.; Kishi, Y.; Hasegawa, T.; Okuzaki, D.; Hirano, T.; Minoshima, M.; Kikuchi, K.; Kumanogoh, A.; Ishii, M. *In vivo* visualisation of different modes of action of biological DMARDs inhibiting osteoclastic bone resorption. *Ann. Rheum. Dis.* **2018**, *77*, 1219−1225.
(42) Mundy, G. R. Metastasis: Metastasis to bone: causes, consequences and therapeutic opportunities. *Nat. Rev. Cancer* **2002**, *2*, 584−593.
(43) Kikuta, J.; Shirazaki, M.; Sudo, T.; Mizuno, H.; Morimoto, A.; Suehara, R.; Minoshima, M.; Kikuchi, K.; Ishii, M. Dynamic analyses of the short-term effects of different bisphosphonates using intravital two-photon microscopy. *JBMR Plus.* **2018**, *2*, 362−366.
(44) Nakamura, I.; Sasaki, T.; Tanaka, S.; Takahashi, N.; Jimi, E.; Kurokawa, T.; Kita, Y.; Ihara, S.; Suda, T.; Fukui, Y. Phosphatidylinositol-3 kinase is involved in ruffled border formation in osteoclasts. *J. Cell. Physiol.* **1997**, *172*, 230−239.

DOI: 10.1021/acscentsci.9b00220
ACS Cent. Sci. 2019, 5, 1059−1066